LA-UR-24-30462

Approved for public release; distribution is unlimited.

Title:	Modelling Beam Loss Within the LANSCE Proton Storage Ring
Author(s):	Yoskowitz, Joshua Tyler; Huang, En-Chuan; Alexander, Anna Marie; Henestroza, Enrique; Xu, Haoran; Taylor, Charles Edward; Lewellen, John Wesley
Intended for:	Report
Issued:	2024-09-30

LANSCE Modernization Project

Modelling Beam Loss Within the LANSCE Proton Storage Ring

J. T. Yoskowitz, E-. C. Huang, A. Alexander, E. Henestroza, H. Xu, C. E. Taylor, and J. W. Lewellen

Report #: LA-UR-24-XXXX
September 27, 2024

Los Alamos National Laboratory

NNSA

Table of Contents

Summary

Several upgrades are being considered for the proton storage ring (PSR) at the Los Alamos Neutron Science Center (LANSCE) to reduce beam loss and thereby reduce the cooldown period of the PSR following a beam run. First, we have considered an increased beam pipe diameter would reduce beam loss due to beam scraping caused by misalignments and tuning errors. However, this would require increased pole-to-pole gap height within the dipoles and quadrupoles, which would change their effective length and alter their fringe fields. The effect of different magnet gaps on the beam optical parameters and on beam loss was studied using the simulation codes MAD-X and PyORBIT. Second, we are developing a detailed particle tracking model within the framework of the simulation package General Particle Tracer (GPT) for the PSR H^- stripping system. This model will be used to study the effect of the stripper foil parameters

(position, composition, areal density, depth, etc.) on first-turn losses, where most of the observed beam loss and emittance growth occurs due to foil scattering, foil stripping, and Lorentz stripping. The model implements C++ custom elements created to model foil scattering, foil stripping, and Lorentz stripping, as these are not built-in features of GPT. The preliminary results of the MAD-X and PyORBIT simulations, as well as the GPT simulation model, is described in this tech note.

1 LANSCE PSR

The LANSCE PSR, shown in Fig. 1, is a 90.2 m ring that accumulates 625 μs pulses of 795 MeV protons from the LANSCE linac into 290 ns proton pulses over ~1745 turns [1]. The resulting 5 nC pulses are then delivered to the Manuel Lujan Neutron Scattering Center and the Weapons Neutron Research (WNR) Facility for spallation neutron experiments [2]. The higher the intensity of the proton pulse, the higher the neutron energy resolution in these experiments [3].

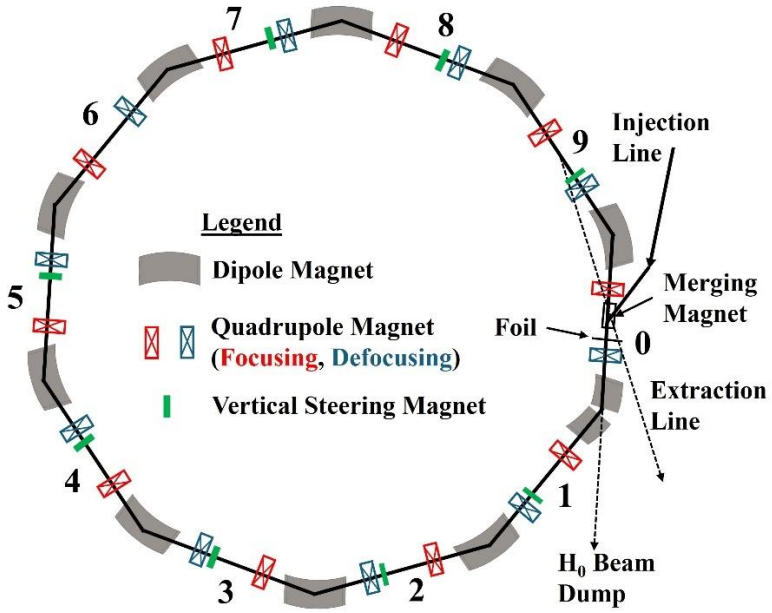

Figure 1 Layout of the PSR depicting the magnetic beamline elements, (dipoles, quadrupoles, vertical steerers), as well as the merging magnet, foil, and the injection and extraction lines. The ten sectors of the PSR are numbered 0 to 9 for reference.

The PSR is composed of ten sectors, each of which is composed of a pair of quadrupoles surrounded by dipoles that bend the beam 36°. That is, each sector is composed of a half-dipole, drift, focusing quadrupole, drift, defocusing quadrupole, drift, and half-dipole. Figure 1 shows a layout of the PSR. Two sectors break the 10-fold symmetry. Sector 0 contains a 6.8° merging magnet to accommodate the injected beam. The two dipoles between sectors 0 and 1 each bend the beam 16.2° to accommodate a beam dump line for H_0. The dipole between sectors 9 and 0 bends the beam 32.8° to accommodate the merging magnet. The accumulated pulse is extracted from the ring using extraction kickers. The design parameters of the PSR are listed in Table 1.

Design Parameter	Value
Beam Kinetic Energy	795 MeV
β (v/c)	0.84
γ (Lorentz Factor)	1.85
Circumference	90.2 m
Nominal Current	100 μA
Rep Rate	20 Hz
Accumulation time	625 μs

Table 1: Design parameters for the PSR.

The maximum pulse intensity that can be achieved by the PSR is limited primarily by beam loss, particularly during the injection process and from emittance growth [4]. Beam losses also lengthen maintenance periods following beam runs, as the protons can activate ring components, resulting the PSR having to "cool down" prior to any hands-on maintenance [5]. Several methods have been proposed to reduce beam loss, including increasing the size of the PSR beam pipe from 4 inches to 6 inches. A larger beam pipe would reduce the recirculating beam loss due to emittance growth, as well as misalignment and tuning errors; however, it would require increasing the pole gaps of the dipoles and quadrupoles, which would alter their effective lengths [6]. Another method to reduce beam loss is to improve the efficiency of the injection system and in particular, the stripping mechanisms that convert the injected H^- beam into H^+ [7].

Detailed simulation models were developed using MAD-X [8] and PyORBIT [9] to study the effects of larger magnet gaps on the optical parameters of the proton beam within the PSR. A separate particle-tracking simulation model of the injection system from the foil to the first dipole downstream of the foil was created using the simulation package GPT [10], with C++ custom elements created and implemented to simulate foil scattering, foil stripping, and Lorentz stripping, to study beam losses within this region. The beam losses within this region are referred to in this paper hereafter as "first-turn losses". The PSR design and the simulation models are described, and the preliminary simulation results are discussed in the following sections.

2 Beam Optics and Loss vs. Magnet Gap

The effect of an increased beam pipe diameter from 4 inches to 6 inches (and the corresponding increased magnet gaps) on the beam optics and beam loss was studied using PyORBIT and MAD-X. PyORBIT is an open-source, particle-in-cell (PIC) code developed at SNS for particle tracking through multiple turns of a circular accelerator or storage ring. MAD-X, on the other hand, is an envelope code developed at CERN for quickly determining the optical parameters along an accelerator beamline and, for a storage ring, finding a periodic solution. A lattice file of the PSR ring used in the MAD-X and PyORBIT simulations was originally developed by J. Kolski in 2011 [11].

Beam Optics vs. Magnet Gap

Figure 2 shows the Courant-Snyder functions in the transverse planes based on a MAD-X simulation of the PSR with a 4-inch beam pipe. The recirculating proton beam undergoes betatron oscillations, one oscillation per PSR sector. When the simulation is repeated for increased beam pipe diameters, the oscillation amplitude increases particularly in the vertical plane, while the frequency of oscillation remains constant, as shown in Fig. 3. Physically, this means that as the pole gap height of the dipoles increases, the effective length of the dipole increases, implying that protons spend more

time in the vertically defocusing fringe fields of the dipoles. The absolute increase in oscillation amplitude compared to the total amplitude is small, so the effect of an increased magnet gap on the optical parameters is likely negligible.

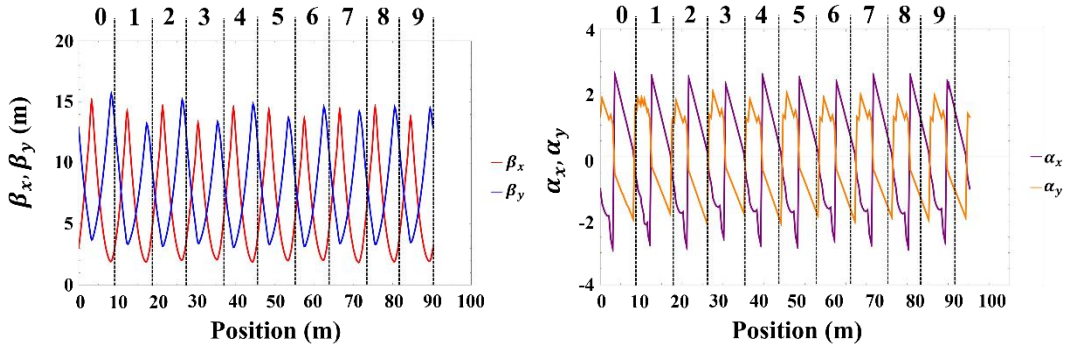

Figure 2: Plots of the optical paramters $\alpha_{(xy)}$ (left) and $\beta_{(xy)}$ (bottom) along the PSR beamline, with the current 4-inch beampipe based on a MAD-X simulation of the PSR. The numbers 0-9 correspond to the PSR sectors in Fig. 1. Position 0 m corresponds to the position of the foil.

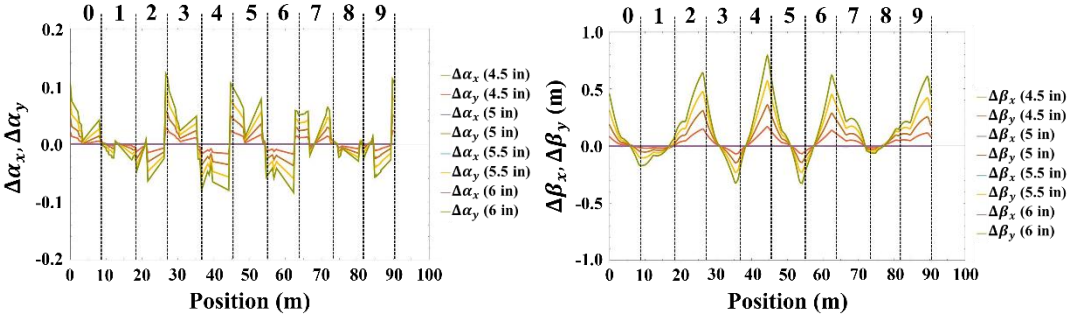

Figure 3:Plots of the absolute difference in $\alpha_{(xy)}$ (left) and $\beta_{(xy)}$ (right) for increased PSR beampipe diameters compared to the values of $\alpha_{(xy)}$ and $\beta_{(xy)}$ for a 4-inch beampipe shown in Fig. 2, based on MAD-X simulations of the PSR. The numbers 0-9 correspond to the PSR sectors in Fig. 1. Position 0 m corresponds to the position of the foil.

Beam Loss vs. Magnet Gap

PyORBIT simulations were used to study beam loss around the PSR for different magnet gaps. In each simulation, 200 H^+ macroparticles, representing the foil-stripped H^- beam with an overall charge of 5 μC, are injected into the PSR every turn and are tracked for a total of 1745 turns. The lattice file used in the MAD-X simulations was adapted for use in the PyORBIT simulations using a built-in MAD-X parser. To model beam loss, apertures were placed at the entrance, center, and exit of every beamline element, including the drift spaces, and the number of particles that hit the apertures were tallied. Figure 4 shows the total beam loss along the PSR ring for beam pipe diameters (and corresponding magnet gaps) between 2 inches and 9 inches. Most of the beam loss for each beam pipe diameter occurs within sector 0 and the first half of sector 1. These first-turn losses are mainly due to scattering within the injection stripper foil, resulting in emittance growth. As the magnet gap decreases, an increasing amount of recirculating beam scrapes the beam pipe around the PSR and is lost. When the magnet gap is increased past 6 inches, the beam loss downstream of the first half of sector 1 becomes negligible and the remaining beam loss is solely from first-turn losses.

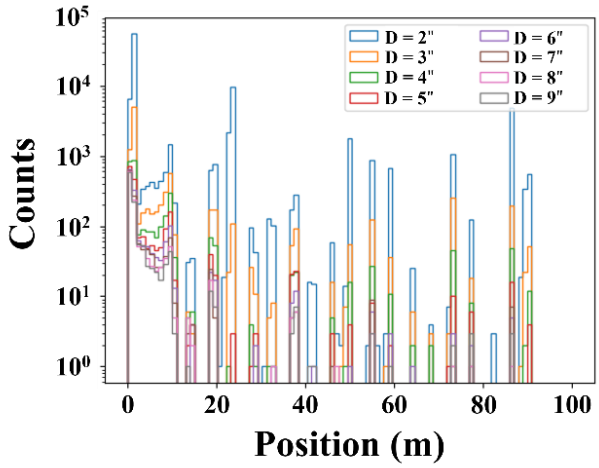

Figure 4: Histograms of the total beam loss around the PSR ring for different beampipe diameters based on PyORBIT simulations of the PSR. Position 0 m corresponds to the position of the foil.

3 PSR Injection System

Figure 5 shows a schematic of the PSR injection system from the merging magnet to the first 16.2° dipole. The field of the merging magnet is such that the injected H^- and the recirculating H^+ beam both bend 6.8° and reach the same location on the stripper foil. The field strength of the merging magnet is about 1.9 kG, which is insufficient to Lorentz strip the H^- ions within the magnet. When the H^- and H^+ beams reach the foil, they both undergo scattering as they pass through the foil. Additionally, the H^- beam is partially stripped into H^+ or H_0 via foil stripping. The resulting H^-, H_0 and H^+ beams pass through a defocusing quadrupole, then a 16.2° dipole magnet, which bends the H^+ into the PSR, while the H_0 passes straight through the dipole to the H_0 beam dump. Any H^- unstripped by the foil will Lorentz strip into H_0 within the magnet. H_0 can Lorentz strip into H^+ within the dipole magnet provided its electron is in the second excited state ($n = 3$) or higher. However, the electron can transition to a lower energy state due to a finite transition lifetime and not undergo Lorentz stripping within the dipole.

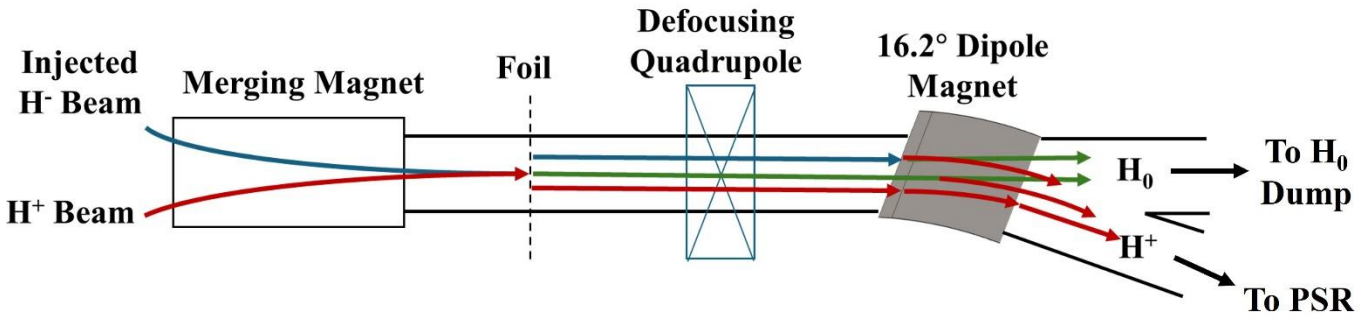

Figure 5: Schematic of the PSR injection system from the merging magnet to after the first 16.2° dipole magnet. The paths of the H^- beam (blue), H_0 beam (green) and H^+ beam (red) are labeled.

4 Simulating First-Turn Losses

A framework for particle tracking simulations of the PSR injection system was developed using the simulation tool GPT to study and predict first-turn losses due to foil scattering, foil stripping, and Lorentz stripping. In each simulation, an 800 MeV H^- beam representing the beam injected into the PSR is tracked from 0.25 m of the stripper foil to 1 m downstream of the dipole. The beam is represented as an H^- bunch composed of 10^4 macroparticles with a total charge

of 1 nC. The bunch has a transverse size of 5 mm (rms) and a length of 1 ns. The recirculating H^+ beam is not included in the simulations. As the H^- beam passes through the foil and dipole magnet, it undergoes foil and Lorentz stripping respectively. The resulting H^-, H_0, and H^+ particles are then tracked until they reach the simulation boundary. The stripper foil is modelled as a thick, infinite plane perpendicular to the z-axis such that the beam is guaranteed to pass through the foil. The foil is centered at z = 0.25 m and is made of pure carbon with an areal density of 450 μg/cm^2 and depth of 1 μm.[1] The dipole magnet is modeled as a rectangular magnet using a built-in GPT element.

Because foil scattering, foil stripping, excited state tracking, and Lorentz stripping are not built-in features of GPT, three C++ custom elements FoilPyORBIT, LifeState, and StripMagnet, were developed and implemented in each simulation. Because each of these processes are probabilistic in nature, each custom element employs one or more Monte Carlo algorithms to determine the populations and distributions of H^-, H_0 (in different excited states), and H^+ in the simulation. The theoretical equations used to simulate foil scattering, foil stripping, and Lorentz stripping are described in Appendix A and the algorithms of the three custom elements are described in Appendix B.

The simulations are bounded by the 4-inch (~0.1 m) diameter PSR beampipe, 0.25 m upstream of the foil (to show the injected H^- beam), and 0.5 m downstream of the dipole magnet. Any particle that reaches the boundary is removed from the simulation. The beampipe corner between the H_0 dump beamline and the PSR sector 1 beamline, however, is not presently included in the simulation. The coordinate system used is such that the z-axis is aligned with the center of the beamline, the y-axis points vertically upward, and the x-axis points to the left when looking downstream. The magnetic field profiles of the quadrupole and dipole magnets used in the simulations are based on built-in GPT elements. Figure 6 shows a schematic of the beamline elements in the simulation model and includes their positions and dimensions, as well as the field strengths of the quadrupole and dipole magnet.

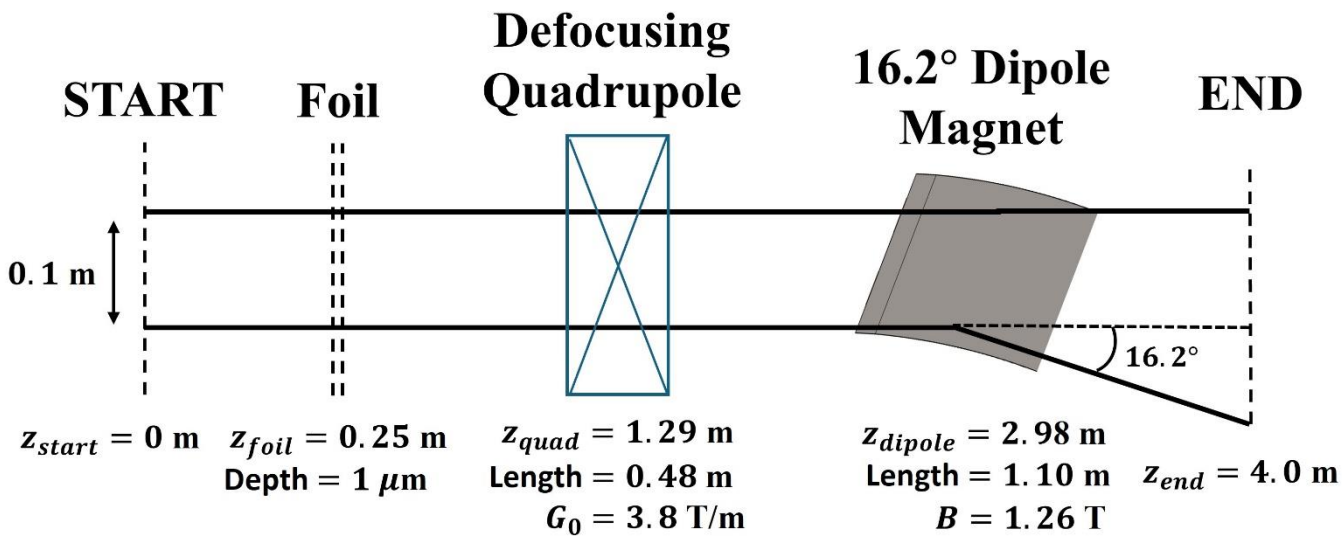

Figure 6: Schematic of the GPT simulation setup, starting from 0.25 m upstream of the foil and ending 0.5 m downstream of the dipole. The positions and lengths of each beamline element are shown, as well as the field strengths of the quadrupole and the dipole.

[1] When describing stripper foils, the term "thickness" is often used in the literature, but it is ambiguous – it usually means the areal density (often in μg/cm^2), but it could also mean the depth (often in m). To avoid confusion, the terms "areal density" and depth" are used instead of "thickness".

5 Simulation Results

Figure 7 shows snapshots of a GPT simulation after 7 ns, 12 ns, and 16 ns. After 7 ns, the H^- bunch has passed through the stripper foil, resulting in the H^- undergoing foil scattering and stripping. After 12 ns, the leading half of the bunch has entered the fringe field of the dipole. Any H^+ created due to foil stripping bends to the right towards sector 1 of the PSR. Some of the H^- ions that were unstripped by the foil, as well as H_0 atoms in the second (or higher) excited state, undergo Lorentz stripping into H^+ and thus bend towards sector 1. H_0 atoms in the ground state or first excited state continue straight through the dipole towards the H_0 beam dump. Finally, after 16 ns, the foil stripped H^+ continues into the PSR while the H_0 continue straight. Some of the H_0 in the third (or higher) excited state undergo Lorentz stripping while within the dipole and begin to bend towards the sector 1. However, these H^+ would likely get lost during recirculation within the PSR, as they are outside the acceptance range of the PSR.

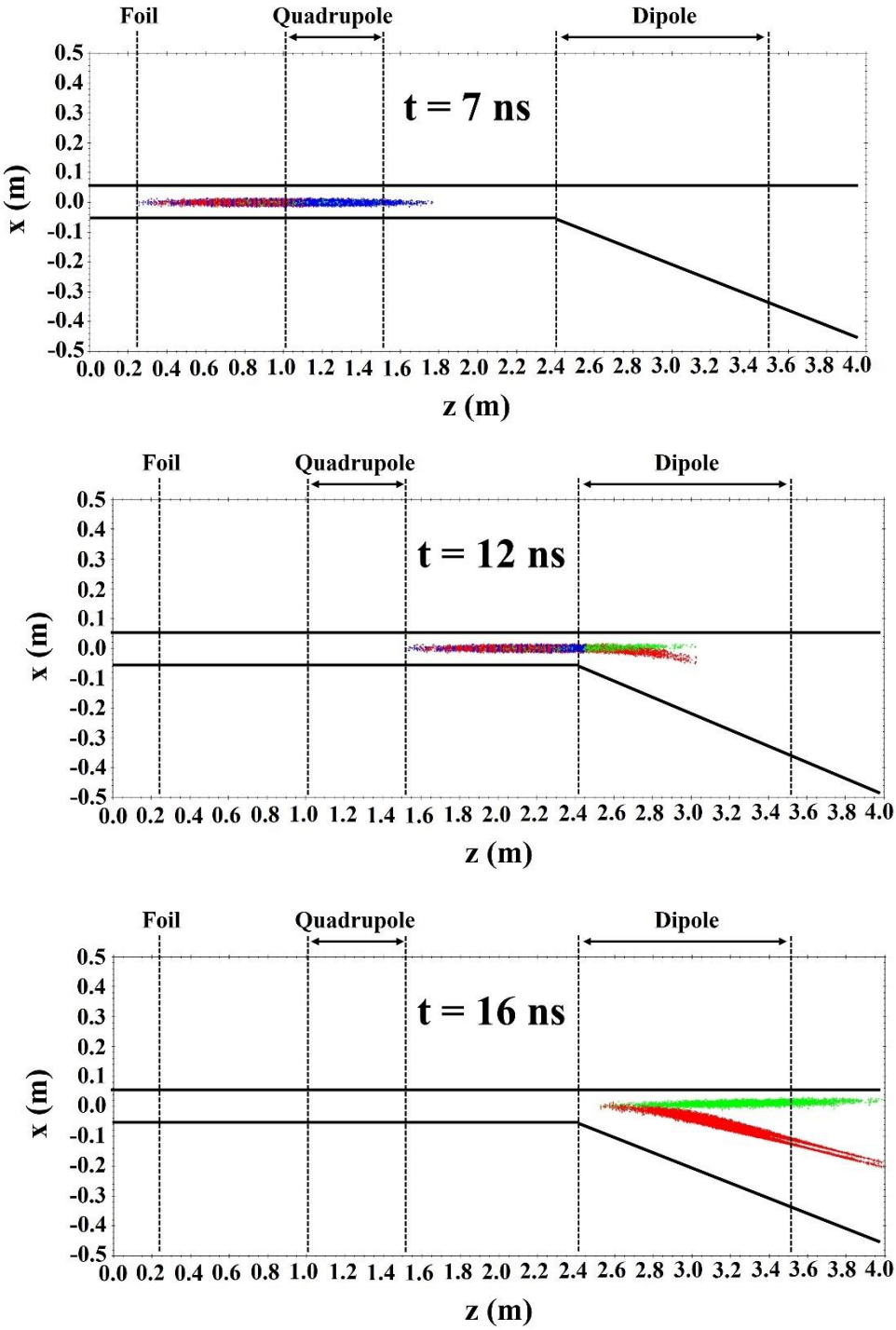

Figure 7: Snapshots of the GPT simulation at t = 7 ns (top), 12 ns (center), and 16 ns (bottom), showing H^- (blue) stripping into H^+ (red) and H_0 (green).

6 Discussion

The beam optics and beam loss within the PSR have been modeled successfully using MAD-X and PyORBIT. The results of the MAD-X simulations show a small increase in the magnitude of the Courant-Snyder α and β functions for larger beam pipe diameters due to the longer effective lengths of the dipole magnets, but this increase is likely negligible. The results of the PyORBIT simulations show most the beam loss occurring in the first several meters downstream of the foil and are likely due to emittance growth as a result of scattering through the foil. The simulations also show beam loss in in the remaining sectors of the PSR. However, this loss can be mitigated with larger beam pipe diameters.

There is ongoing work to improve the accuracy and sophistication of the GPT simulation model of first-turn losses. As the custom elements are developed, there are plans to benchmark the simulation results against other simulation codes such as PyORBIT, Xsuite [12], and MCNP [13], as well as against experimental data. In addition, magnetic models of the dipoles and quadrupoles are being developed using CST software [14] to accurately determine the fringe fields.

Acknowledgements

The team expresses deep gratitude to the NNSA Office of Experimental Sciences, for their investments in advancing capabilities and tools for this work.

Appendix A: Foil and Lorentz Scattering Theory

The following subsections describe theory of foil scattering, foil stripping, and Lorentz stripping.

Foil Scattering

When H^- and H^+ ions pass through a stripper foil, they scatter off atoms in the foil, as shown in Fig. [Foil Scatter Diagram]. Their resulting transverse momentum distributions depend on the initial momenta of the H^- and H^+ ions, and the properties of the foil, including its elemental composition, its areal density, and depth. PyORBIT models foil scattering using two routines, named “simple” and “full”. The “simple” routine uses simplified multiple Coulomb scattering (MCS) theory to calculate the transverse kicks from each atom the ion scatters off within the foil. The “full” routine considers both MCS and nuclear elastic and inelastic scattering cross sections based on MCNP. Both PyORBIT routines are summarized here.

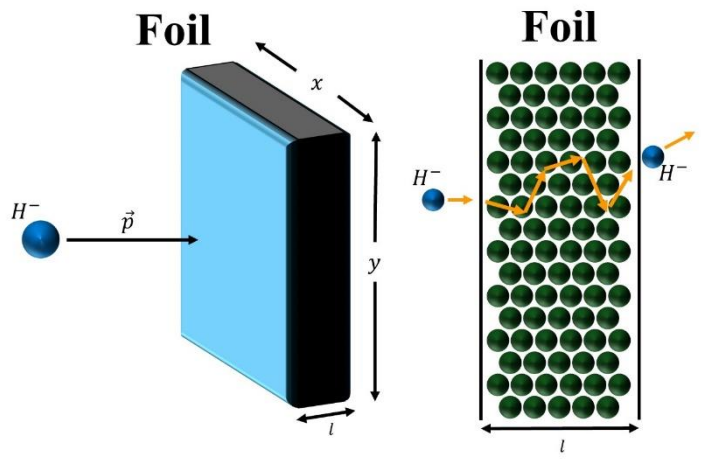

Figure 8: Diagram of an H- incident on a foil (left). The H- ion scatters off atoms as it passes through the foil (right).

Simple Foil Scattering Algorithm

The simple scatter routine tracks an incident H- it passes through a rectangular foil. The routine follows the theory described in section 13.6 of Jackson [15], and we refer the reader to that section for a more detailed description.

First, the momentum p of the incident H- ion is calculated:

$$p = m\gamma\beta c \tag{1}$$

where m is the mass of H-, γ and β are the relativistic factors, and c is the speed of light. The minimum and maximum scattering angles, between which the Coulomb-field approximation holds, are calculated based on Eqs. 13.101 and 13.102 in Jackson [15]:

$$\theta_{min} = \frac{\hbar}{pR_{TF}} \tag{2}$$

$$\theta_{max} = \frac{\hbar}{pR} \tag{3}$$

$$R_{TF} = 1.4 r_{Bohr} Z^{-\frac{1}{3}} \tag{4}$$

$$R = \frac{e^2 a^{\frac{1}{3}}}{2mc^2} \approx 1.4 \times 10^{-13} a^{\frac{1}{3}} \text{ cm} \tag{5}$$

where R_{TF} is the atomic radius in the Thomas-Fermi model, Z and a are the atomic number and weight of the foil material element, and $r_{bohr} = \frac{\hbar^2}{m_e e^2}$ is the Bohr radius.

The transverse kicks x′ and y′ are then calculated:

$$\theta = \theta_{min} \sqrt{\frac{n_{rand}}{1 - n_{rand}}} \tag{6}$$

$$\theta_x \mathrel{+}= \theta \cos\phi \tag{7}$$

$$\theta_y \mathrel{+}= \theta \sin\phi \tag{8}$$

$$x' \mathrel{+}= \theta_x \tag{9}$$

$$y' += \theta_y \tag{10}$$

where n_{rand} is a random number between 0 and 1 and ϕ is a random angle between 0 and 2π. If $\theta > 2\theta_{max}$, the θ is set to $2\theta_{max}$ to prevent unrealistic scattering angles.

Full Foil Scattering Algorithm

The full scatter routine is similar to the simple scatter routine, but also takes into account nuclear scattering using elastic and inelastic cross sections from MCNPX. It can also remove the particle if it undergoes nuclear inelastic absorption. The routine first calculates the total Rutherford scattering cross section using Eq. 13.104 in Jackson [15]:

$$\sigma_R = \pi r_{min}^2 \left(\frac{2zZe^2}{\hbar\beta c}\right)^2 = \frac{\pi}{\theta_{min}^2}\left(\frac{2zZe^2}{pv}\right)^2 \tag{11}$$

where $r_{min} = 1.4a^{-\frac{1}{3}} \times 10^{-15}$ m and $z = 1$ is the atomic number for H^-. Note that the Rutherford cross section is cut off at θ_{min}, as the true total Rutherford cross section diverges.

The elastic and inelastic cross sections are derived from MCNPX and are functions of the particle energy. PyORBIT's `cross_sections.cc` file contains lists of cross sections for each supported foil material, as well as a list of energies in GeV, ranging from 0.5 MeV to 2.5 GeV over 59 (non-equally spaced) values. The cross sections for a given individual particle energy are derived using linear interpolation between closest values. Fig. 11 shows the elastic and inelastic cross sections for each supported foil material. Both elastic and inelastic scattering cross sections are roughly constant at energies above 400 MeV for each foil material, implying that the choice of foil material (and hence the atomic density within the foil) has the greatest impact on the scattering cross section.

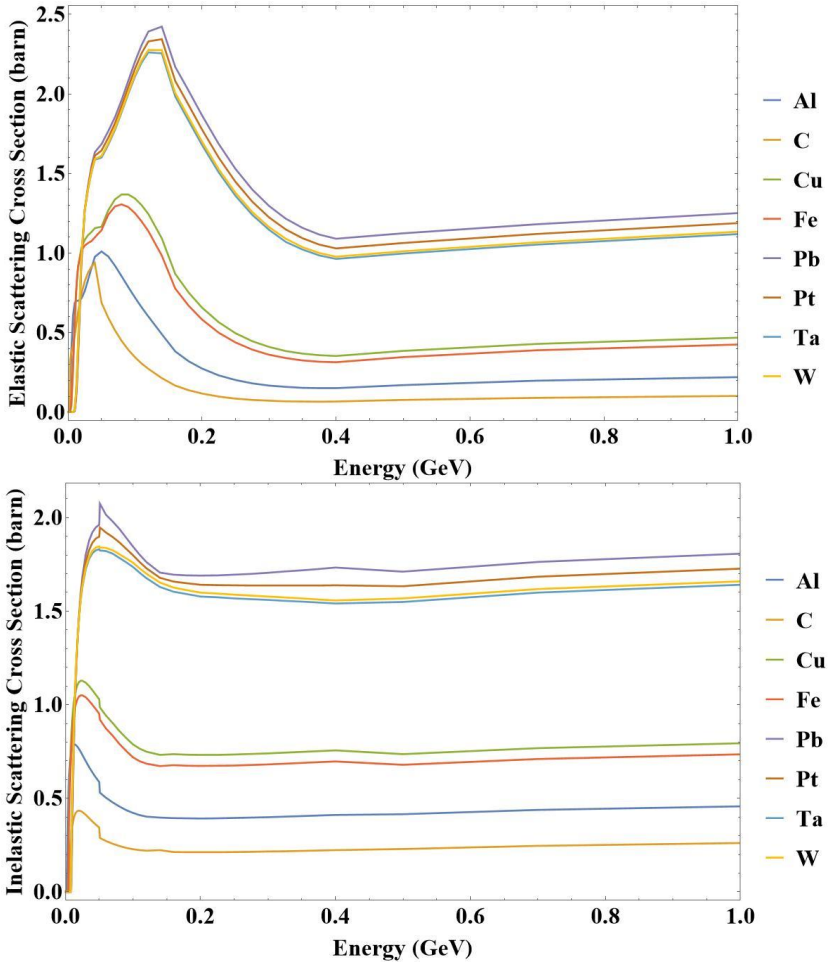

Figure 9: Elastic (Top) and inelastic (Bottom) scattering cross sections as a function of incident H- energy for different foil materials.

As the H^- ion passes through the foil, it scatters off multiple foil atoms. The total number of Coulomb collisions per unit depth $\frac{n}{t}$ is given by:

$$n = N\sigma_R t$$

The final transverse momenta of the ion, x'_f and y'_f, upon exiting the foil are given by:

$$x'_f = \tan\left[\arctan(x'_i) + \cos(2\pi n_{rand,1})\sqrt{-\frac{2n\ln(n_{rand_2})\ln\left(\frac{\theta_{max}}{\theta_{min}}\right)}{\frac{1}{\theta_{min}^2}-\frac{1}{\theta_{max}^2}}}\right] \quad (12)$$

$$y'_f = \tan\left[\arctan(y'_i) + \sin(2\pi n_{rand,1})\sqrt{-\frac{2n\ln(n_{rand_2})\ln\left(\frac{\theta_{max}}{\theta_{min}}\right)}{\frac{1}{\theta_{min}^2}-\frac{1}{\theta_{max}^2}}}\right] \quad (13)$$

where $n_{rand,1}$ and $n_{rand,2}$ are random numbers between 0 and 1.

With every collision, the H^- ion loses energy. The average energy loss per unit length within the foil is given by the Bethe-Block equation, the form of which can be found in Eq. 34.5 in the Particle Data Group (PDG) book on the Review of Particle Physics (2022) [16]:

$$\langle -\frac{dE}{dx} \rangle = \frac{Kz^2 Z}{a\beta^2}\left[\frac{1}{2}\ln\left(\frac{2m_e c^2\beta^2\gamma^2 T_{max}}{I^2}\right) - \beta^2 - \frac{\delta(\beta\gamma)}{2}\right] \tag{14}$$

$$T_{max} = \frac{2m_e c^2\beta^2\gamma^2}{1 + \frac{2\gamma m_e}{M} + \left(\frac{m_e}{M}\right)^2} \tag{15}$$

$$K = 4\pi N_A r_e^2 m_e c^2 \tag{16}$$

$$r_e = \frac{e^2}{4\pi\epsilon_0 m_e c^2} \tag{17}$$

where m_e is the electron mass, M is the mass of a foil atom, N_A is Avogadro's number and r_e is the classical electron radius. The factor I is the mean excitation energy, with empirically derived values for different elements tabulated by NIST, e.g. [17], with references therein. T_{max} is the maximum kinetic energy transfer to an electron in the target atom in a single collision. The term $\delta(\beta\gamma)/2$ is the so-called density-effect correction for highly relativistic particles ($\beta\gamma \gg 2$) passing through dense media. This term is neglected in PyORBIT and in the FoilPyORBIT custom element and we refer the reader to Jackson Section 13.4 for a detailed discussion of the density-effect correction [15].

Equations (12) and (13) do not take into account nuclear elastic scattering. The corrections to the transverse kicks are calculated as follows: the center-of-mass momentum p_{CM} between the incident H^- ion and the target atom (assumed to be at rest) is:

$$p_{CM} = p\left(\frac{Mc^2}{\sqrt{(pc)^2 + (mc^2)^2}}\right) \tag{18}$$

The elastic scattering angle θ_E is:

$$\theta_E = 2p_{CM}(1 - \cos(2\pi n_{rand})) \tag{19}$$

where n_{rand} is a random number between 0 and 1. The correction to the transverse kicks are then:

$$x'_{f,E} = x'_f + \arccos\left(1 - \frac{\theta_E}{2p}\right)\left(\frac{2v_a v_b}{v_a^2 + v_b^2}\right) \tag{20}$$

$$y'_{f,E} = y'_f + \arccos\left(1 - \frac{\theta_E}{2p}\right)\left(\frac{v_a^2 - v_b^2}{v_a^2 + v_b^2}\right) \tag{21}$$

$$v_a = 2n_{rand} - 1,\ v_b = n_{rand} - 1,\ v_a^2 + v_b^2 \leq 1$$

Foil Stripping

As H^- scatters through the foil, one or both electrons can be stripped. Following the theory described by Mohagheghi et al. [18] and Gervais, Reinhold, and Burgdörfer [19], the probability of H^- stripping into either H_0 or H^+ at a foil depth t is given by:

$$P_{-0+} \equiv 1 - e^{\rho\sigma_- t} \tag{22}$$

where $\sigma_- = \sigma_{-0} + \sigma_{-+}$ is the total cross section, σ_{-0} and σ_{-+} are the cross sections for stripping into H_0 and H^+ respectively, and ρ is the foil density in atoms per microgram.

When H^- strips into H_0, the remaining electron can be in an excited state. For example, the probability of an H^- stripping into an H_0 in the $n = 1$ (ground) state or $n = 2$ state at a foil depth t is [20]:

$$P_{12} \equiv \frac{\sigma_{-12}}{\sigma_- - \sigma_{12}}(e^{-\sigma_{12}\rho t} - e^{\sigma_- \rho t}) \tag{23}$$

where σ_{-12} is the cross section for H^- stripping into the $n = 1$ or $n = 2$ state and σ_{12} is the cross section for excitation of H_0 in the 1 or 2 state into a higher excited state. The probability of H^- stripping into H_0 in a higher excited state ($n \geq 3$) is [20]:

$$P_{n>3} \equiv A_1 e^{-\rho\sigma_- t} + A_2 e^{-\rho\sigma_{12} t} - (A_1 + A_2)e^{-\rho\sigma_n t} \tag{24}$$

$$A_1 \equiv \frac{\sigma_{-n} - C\sigma_{12n}}{\sigma_n - \sigma_-}$$

$$A_2 \equiv \frac{C\sigma_{12n}}{\sigma_n - \sigma_{12}}$$

$$C = \frac{\sigma_{-12}}{\sigma_- - \sigma_{12}}$$

where σ_n is the cross section for H_0 excitation from state n into any other state and σ_{12n} is the cross section for H_0 excitation from the $n = 1$ or $n = 2$ state into state n.

Equations (22)-(24) imply that the likelihood of H^- stripping into either H_0 or H^+ increases exponentially with the foil depth t. Thus, the thicker the stripper foil, the less likely H^- would remain unstripped after passing through the foil. The trade-off is the thicker the stripper foil, the higher the number of scatters of the H^- within the foil, resulting in a H^+ beam with an increased emittance and reduced kinetic energy following the foil.

Lorentz Stripping

Charged particles passing through a transverse magnetic field $B_\perp$ experience an equivalent transverse electric field in the rest frame of the particles, given by [21]:

$$E_\perp = 0.3\beta\gamma B_\perp \times 10^6 \frac{\text{V}}{\text{cm}} \tag{25}$$

where $B_\perp$ is in units of kilogauss. The relativistic factors β and γ imply that $E_\perp$ is significant only at relativistic speeds. For example, if an 800 MeV H^- ion ($\beta = 0.84, \gamma = 1.85$) passes through a 10 kG dipole magnet, it experiences an equivalent electric field of 4.66 MV/cm. Given that the binding energy of the second electron of an H^- atom is about 0.755 eV, a sufficiently high magnetic field can strip the H^- to H_0, a process known as Lorentz stripping. As an H^- passes through a dipole magnet, the probability of Lorentz stripping P_L within a distance d is [22]:

$$P_L = \frac{Bd}{k_1} e^{-\frac{k_2}{\beta\gamma cB}} \tag{26}$$

$$k_1 = 2.47 \times 10^{-6}\ \text{sV/m}$$

$$k_2 = 4.49 \times 10^9\ \text{V/m}$$

where k_1 and k_2 are fitting parameters given by Jason, Hudgings, and van Dyck [23]. Given a dipole magnet of sufficient magnetic field strength and (effective) length, a relativistic H^- ion almost certainly strips to an H_0 by the time it exits the magnet. H_0 can also strip to H^+ depending on the energy state of the electron and given a sufficiently high magnetic field strength.

H^- can also undergo Lorentz stripping when passing through a quadrupole magnet. The main difference between quadrupoles and dipole magnets is that the magnetic field has radial dependence. Because $B_\perp$ increases with increasing radial distance r from the central axis. From Eq. (26), this implies that H^- and H_0 in excited states are more likely to undergo Lorentz stripping when in the outer beam halo, or when the beam itself is misaligned with the central axis. Folsom *et al.* shows in Figs. 8 and 9 in Ref. [22] that Lorentz stripping within a quadrupole magnet is proportional to the transverse

beam size and inversely proportional to the field gradient; the latter is due to particles in the beam halo being closer to the quadrupole poles when the gradient is low and hence experiencing increased Lorentz stripping.

Figure 1 in Yamane [24] suggests that Lorentz stripping of H_0 in the ground state requires a magnetic field strength on the order of hundreds of kilogauss, which is well above the magnetic field strength of the PSR dipole magnets. However, if the H_0 were in an excited state of $n = 3$ or higher, the field strengths of the PSR dipoles would be sufficient to strip the H_0 into H^+.

As mentioned earlier, the stripper foil can strip an H^- into an H_0 in an excited state. However, the lifetime of the excited state is finite. The probability P_{trans} that an H_0 in an excited state will transition from the $n = i$ state to the $n = j < i$ state within a timestep Δt is given by an exponential decay law:

$$P_{trans} = 1 - \exp\left(-\frac{\Delta t}{\tau_{ij}}\right) \tag{27}$$

where τ_{ij} is the transition lifetime. Transition rates $1/\tau_{ij}$ for H_0 up to $n = 6$ are given by NIST [25], and range from a few kilohertz to several hundred megahertz, implying lifetimes on the order of milliseconds to nanoseconds. It is worth noting that the cross section for H^- foil stripping into H_0 in a lower excited state ($n = 1$ or $n = 2$) is one to two orders of magnitude higher than stripping into a higher excited state ($n \geq 3$), and the transition lifetimes between lower excited states is orders of magnitude shorter than between higher excited states. These two facts imply that when an 800 MeV H^- strips into H_0, it is likely in a lower excited state and will decay to the ground state within a meter after the foil.

Appendix B: FoilPyORBIT, LifeState, and StripMagnet Algorithms

The algorithms used in the GPT custom elements FoilPyORBIT, LifeState, and StripMagnet are described in the following subsections.

FoilPyORBIT

The FoilPyORBIT custom element, named because its foil scattering algorithm is based on PyORBIT's algorithm described in the appendix, can be used in a GPT simulation to simulate foil scattering and foil stripping. The custom element models a stripper foil, represented by an infinite plane perpendicular to the z-axis at $z = 0$. Future updates to the element will permit the user to specify the edges of the foil in the x and y directions. The custom element requires several user-defined parameters listed below:

1. The user can choose the position and orientation of the foil by adjusting its element coordinate system (ECS). The default position is perpendicular to the z-axis at $z = 0$ (i.e. the xy-plane).
2. The user specifies the foil material, assumed to be composed of exactly one element with uniform density. Currently supported elements are C, Al, Fe, Cu, Ta, W, Pt, and Pb.
3. The user specifies which foil scattering algorithm is used, simple or full, as described in the appendix.
4. If the full scattering algorithm is chosen, the user specifies a separate data file containing elastic and inelastic cross section data for the specified foil material. This data file must be a GDF file (GPT data file) containing three arrays: kinetic energy, elastic cross section (in cm^2), and inelastic cross section (in cm^2). PyORBIT contains elastic an inelastic cross section data for each supported element based on MCNPX in its cross_sections.cc file. These were converted into GDF files for the GPT simulations.
5. The user can optionally switch off foil stripping in order to only simulate foil scattering.
6. The user specifies the areal density of the foil. The use can specify the foil depth only if the full scatter algorithm is chosen, as the simple scatter algorithm assumes the foil is infinitely thin.
7. The user specifies particle set names for H^-, H_0 and H^+. These set names should be consistent throughout the GPT input file used for the simulation.

GPT tracks simulated macroparticles over timesteps. Each macroparticle represents some number of elementary particles (protons, electrons, etc.). FoilPyORBIT loops over all macroparticles currently present in the simulation in each timestep. A macroparticle is eligible for foil scattering and foil stripping if all the following are true:

1. The macroparticle is in the H^- particle set,
2. The macroparticle does not hit the simulation boundary, and
3. The macroparticle crosses the foil (simple scatter algorithm) or is within the foil (full scatter algorithm).

FoilPyORBIT then calculates the number of stripped H^- for each H^- macroparticle using the formulas:

$$N_{-+} = D\sigma_{-+}n_{macro} \tag{28}$$

$$N_{-0} = D\sigma_{-0}n_{macro} \tag{29}$$

where D is the foil density in atoms per cubic meter and n_{macro} is the number of H^- ions this macroparticle represents. If N_{-+} or N_{-0} are between 0 and 1, a Monte Carlo approach is used: a random number between 0 and 1 is generated. If the random number is greater than N_{-+}, then N_{-+} is set to 0, otherwise it is set to 1. A similar approach is used for N_{-0}.

The number of unstripped H^- is thus:

$$N_{-} = n_{macro} - N_{-+} - N_{-0} \tag{30}$$

Because the foil density can be made arbitrarily high by the user-defined parameters, it is possible that $N_{-} < 0$, which is nonphysical. In this case, N_{-+} and N_{-0} are re-normalized as follows:

$$N_{-+,new} = \frac{n_{macro}N_{-+}}{N_{-+} + N_{-0}} \tag{31}$$

$$N_{-0,new} = \frac{n_{macro}N_{0}}{N_{-+} + N_{-0}} \tag{32}$$

with no H^- left unstripped in this timestep.

If $N_{-0} > 0$, then the number of H^- stripped to each of the first 5 energy states ($1 \leq n \leq 6$) of H_0 are calculated:

$$N_{-0,1} = N_{-0}P_{-0,1} \tag{33}$$

$$N_{-0,2} = N_{-0}P_{-0,2} \tag{34}$$

$$N_{-0,3} = N_{-0}P_{-0,3} \tag{35}$$

$$N_{-0,4} = N_{-0}P_{-0,4} \tag{36}$$

$$N_{-0,5} = N_{-0}P_{-0,5} \tag{37}$$

where $P_{-0,n}$ is the probability of H^- stripping to H_0 in the nth state. $P_{-0,n}$ is calculated using cross sections that are normalized into weights that add up to 1:

$$P_{-0,n} = \frac{\sigma_{-0,n}}{\sigma_{tot}} \tag{38}$$

$$\sigma_{tot} = \sigma_{-0,1} + \sigma_{-0,2} + \sigma_{-0,3} + \sigma_{-0,4} + \sigma_{-0,5} \tag{39}$$

Measured cross sections $\sigma_{-0,n}$ can be found in Table II in M. Gulley *et al*. [17]. Also, note that this tacitly assumes that H_0 can only be in the first 5 energy states, as cross section data in the cited table are only given for the first 5 excited states. For simulation purposes, this is sufficient, as the stripping cross section decreases by orders of magnitude for each higher excited state.

Provided foil stripping is turned on, macroparticles representing stripped H^+ and H_0 in each excited state are added to the simulation. Their n_{macro} values are based on the applicable value of N_{-x} and their momenta are based on the chosen

foil scatter algorithm and is calculated based on the equations described in the previous sections. The excited state of H_0 is kept as a parameter to be tracked by LifeState custom element, described in the next section.

The n_{macro} parameter of the original H^- macroparticle is then reduced by the sum of N_{-+} and N_{-0}. If the resulting n_{macro} is zero, then the H^- is removed from the simulation. Otherwise, it receives a transverse kick according to the chosen scatter algorithm. This transverse kick is still calculated if foil stripping is turned off.

LifeState

The custom element LifeState tracks the excited state of H_0 and transitions the H_0 to a lower excited state according to its lifetime. The lifetimes of all possible transitions between excited states are given by NIST [22], and are stored in the custom element for reference. Lifestate takes two user parameters: the ECS (for purposes of outputting transition info), and the H_0 particle set name.

Whenever a macroparticle is added to the simulation (i.e. during foil stripping from FoilPyORBIT or Lorentz stripping from StripMagnet), LifeState determines the excited state of the macro particle and maps it onto a three-digit number where each digit represents the energy state (1-5), orbital (1=s, 2=p, 3=d, 4=f, 5=g) and spin (1=1/2, 2=3/2, 3=5/2, 4=7/2, 5=9/2). For example, the number 321 implies the H_0 is in the $3p_{1/2}$ state.

In every successful timestep, LifeState determines whether each H_0 present in this timestep (and has not hit the simulation boundary) transitions to a lower excited state using a Monte Carlo approach. LifeState calculates P_{trans} for each H_0 using Eq. (27). The lifetime value used in Eq. (27) is randomly chosen from the allowed transitions based on the current H_0 excited state. LifeState then generates a random number between 0 and 1. If the random number is less than or equal to P_{trans}, the H_0 transitions to the lower excited state based on the chosen lifetime. H_0 ions in the ground state cannot transition, since they are already in the lowest energy state.

LifeState also adds an array to the GPT output file (regardless of whether the output file is time-based or screen-based) called "state", so that the populations of all excited states of H_0 at every timestep can be recorded for analysis

StripMagnet

The custom element StripMagnet is based on the built-in rectangular magnet (`rectmagnet`) and quadrupole (`quadrupole`) GPT elements. StripMagnet extends the functionality of these elements by allowing H^- ions and H_0 atoms (in excited states) to undergo Lorentz stripping while within the boundaries (i.e. the effective length) of the magnet.

Strip magnet requires several user parameters listed below:

1. The user specifies the ECS of the magnet in order to position and orient the magnet in the simulation.
2. The user specifies the kind of magnet to use: dipole or quadrupole. The magnet type chosen determines the next several parameters:
    a. Dipole
        i. The user specifies the dimensions of the magnet (in meters) in the x- and z- directions. The resulting B-field is in the y- direction.
        ii. The user specifies the maximum B-field (in tesla) within the magnet.
        iii. The user specifies a fringe field offset parameter d_l (in meters), typically zero, that can alter the effective length of the magnet, if needed.
        iv. The user specifies the first two Enge coefficients b_1 and b_2 that are used to determine the shape of the fringe fields. The on-axis Enge function is:

$$B_y(z, y = 0) = \frac{1}{1 + \exp(b_1(z - d_l) + b_2(z - d_l)^2)}$$

b_1 is typically $2/g$ where g is the pole gap length and b_2 is typically zero.

b. Quadrupole
   i. The user specifies the quadrupole effective length (in meters).
   ii. The user specifies the nominal field gradient, in Tm^{-1}.
   iii. The user specifies the first Enge coefficient b_1, typically equal to π/r_{bore}, where r_{bore} is the inner radius of the quadrupole.

3. The user specifies the particle set names for H^-, H_0, and H^+.
4. The user optionally specifies the stripped electron particle set name. Specifying the electron set name "turns on" stripped electrons in the simulation so that their particle trajectories can be tracked. The Lorentz stripping algorithm is not affected.
5. The user specifies the fit parameters k_1 and k_2, which are used to calculate the Lorentz stripping probability (see Eq. (26)).

In every GPT timestep, StripMagnet loops over all macroparticles present in the simulation. A macroparticle is eligible to ionize if it is not removed in this timestep, it is in the H^- or H_0 particle set, and the center of its trajectory in this timestep is within the bounds of the magnet (note that the extent of the fringe field is included in this calculation). If it is in the H_0 particle set, then it must be in an energy state of $n = 3$ or higher to undergo Lorentz stripping. Future updates will allow H_0 in the $n = 1$ or 2 state to be considered for Lorentz stripping.

It then calculates the probability P_L using Eq. (26). If $P_L > 1$, the entire timestep is repeatedly failed and retried with shorter timesteps until $0 \leq P_L \leq 1$. A Monte Carlo approach is then taken: if a generated random number between 0 and 1 is less than or equal to P_L, the macroparticle undergoes Lorentz stripping. If stripped electrons are turned on, then an electron with a random fraction of the macroparticle's kinetic energy and a random direction is placed in a random location along the macroparticle's trajectory. If the macroparticle is H^-, it strips to an H_0 in a random excited state. Future updates will consider stripping cross sections into different excited states when the corresponding experimental data becomes available. If the macroparticle is H_0, it strips into H^+.

References

[1] G. P. Lawrence, R. A. Hardekopf, A. J. Jason, B. Blind, and T. W. Hardek, "Proton Storage Ring Commissioning at LANSCE", in *Proc. ICANS IX*, Villingen, Germany, Sept. 1986, pp. 85-99.
[2] R. C. Haight, "Nuclear Data Research at the Los Alamos Neutron Science Center", in *Proc. ND 2007*, Nice, France, Apr. 2007, pp. 415-420, https://doi.org/10.1051/ndata:07515
[3] R. K. Cooper and G. P. Lawrence, "The Design of the WNR Proton Storage Ring Lattice", *IEEE Trans. Nucl. Sci.*, vol. NS-24, no. 3, pp. 1037-1039, June 1977, https://doi.org/10.1109/TNS.1977.4328843
[4] R. J. Macek, D. H. Fitzgerald, M. Hoehn, R. Ryder, and R. York, "Status of the PSR Improvement Program", in *Proc. PAC 93*, Washington D. C., USA, May 1993, pp. 3739-3741.
[5] R. Hutson and R. Macek, "First-Turn Losses in the LAMPF Proton Storage Ring (PSR)", in *Proc. PAC93* Washington D. C., USA, May 1993, pp. 363-365, https://doi.org/10.1109/PAC.1993.308913
[6] J. T. Yoskowitz and E-. C. Huang, "Beam Optics Studies for Larger Beampipe Diameters for the LAMP-PSR", LANL, Los Alamos, NM, USA, Rep. PSR-23-0009, Sep. 2023.
[7] A. Alexander *et al*., "Improved Modelling and Characterization of the LANSCE Stripper Foils", in *Proc. IPAC'24*, Nashville, TN, USA, May 2024, pp. 1722-1725
[8] MAD-X, https://madx.web.cern.ch/madx/
[9] PyORBIT v3, https://github.com/PyORBIT-Collaboration/PyORBIT3
[10] GPT, https://pulsar.nl/gpt/
[11] J. Kolski, "Lattice Modeling and Application of Independent Component Analysis to High Power, Long Bunch Beams in the Los Alamos Proton Storage Ring", Ph. D. thesis, Phys. Dept., Indiana University, Bloomington, IN, 2010.
[12] Xsuite, https://xsuite.readthedocs.io/en/latest/
[13] MCNP, https://mcnp.lanl.gov/

[14] CST Studio Suite, https://www.3ds.com/products/simulia/cst-studio-suite
[15] J. D. Jackson, "Collisions between Charged Particles, Energy Loss, and Scattering", in *Classical Electrodynamics*, New York, NY, USA: Wiley, 19621, pp. 429-462.
[16] R. L. Workman *et al.* (Particle Data Group), "Review of Particle Physics", *Progress of Theoretical and Experimental Physics*, vol 2022, no. 8, Aug. 2022, https://doi.org/10.1093/ptep/ptac097
[17] J. H. Hubbell and S. M. Seltzer, "X-Ray Mass Attenuation Coefficients", *NIST Standard Reference Database 126*, 2004, https://physics.nist.gov/PhysRefData/XrayMassCoef/tab1.html
[18] A. H. Mohagheghi *et al*., "Interaction of Relativistic H^- Ions With Thin Foils", *Phys. Rev. A*, vol. 43, no. 3, pp. 1345-1365, Feb. 1991, https://doi.org/10.1103/PhysRevA.43.1345
[19] B. Gervais, C. O. Reinhold, and J. Burgdörfer, "Simulation of Excited-State Formation of Hydrogen in Transmission of Relativistic H^- Ions Through Thin Foils", *Phys. Rev. A*, vol. 53, no. 5, pp. 3189-3200, May 1996, https://doi.org/10.1103/PhysRevA.53.3189
[20] M. Gulley *et al*., "Measurement of H^-, H^0, and H^+ Yields Produced by Foil Stripping of 800 MeV H^- Ions", *Phys. Rev. A*, vol. 53 no. 5, pp. 3201-3210, May 1996, https://doi.org/10.1103/PhysRevA.53.3201
[21] G. M. Stinson, *et al.*, "Electric Dissociation of H^- Ions by Magnetic Fields", *Nucl. Instr. Meth.*, vol. 74, no. 2, pp. 333-341, Oct. 1969, https://doi.org/10.1016/0029-554X(69)90359-0
[22] B. T. Folsom, M. Eshraqi, N. B. Kraljevic, and B. Gålnander, "Stripping Mechanisms and Remediation for H^- Beams", *Phys. Rev. Accel. Beams*, vol. 24, no. 7, p. 074201, Jul. 2021, https://doi.org/10.1103/PhysRevAccelBeams.24.074201
[23] A. J. Jason, D. W. Hudgings, and O. B. van Dyck, "Neutralization of H^- Beams by Magnetic Stripping", *IEEE. Trans. Nucl. Sci.*, vol 28, no. 3, pp. 2703-2706, Jun. 1981, https://doi.org/10.1109/TNS.1981.4331890
[24] I. Yamane, "H^- Charge-Exchange Injection Without Hazardous Stripping Foils", *Phys. Rev. ST. Accel. Beams*, vol. 1, no. 5, p. 053501, Sept. 1998, https://doi.org/10.1103/PhysRevSTAB.1.053501
[25] J. Baker, "Transition Probabilities for One Electron Atoms", Gaithersburg, MD, USA, Rep. NIST Technical Note 1612, 2008, https://nvlpubs.nist.gov/nistpubs/Legacy/TN/nbstechnicalnote1612.pdf